ECTI Transactions on Computer and Information Technology
Journal homepage: https://ph01.tci-thaijo.org/index.php/ecticit/
Published by the ECTI Association, Thailand, ISSN: 2286-9131

Application of Novel Improved Firefly Algorithm for Image Fusion to Detect Brain Tumor

M. V. Srikanth[1], V. V. K. D. V. Prasad[2] and K. Satya Prasad[3]

ABSTRACT

Image fusion is a method for merging vital elements from two images for higher visual appeal and a better understanding of the data contained in source images. Application areas for image fusion include the military, space exploration, and healthcare. In this study, an attempt is made to use the successful fusion of two images to diagnose brain diseases such as neoplastic tumors, cerebrovascular tumors, Alzheimer's tumors, fatal tumors, and sarcoma tumors. In this case, two images are fused after being segmented with the optimal thresholds obtained using a novel improved Firefly (pFA) algorithm with a maximization problem employing fuzzy entropy as the objective function. These segmented images are then applied to Scale Invariant Feature Transform ($SIFT$) for additional deep feature extraction. Improved features for better fusion can be obtained by this cascaded feature extraction. Finally, fusion rules for the source images are created using interval type-2 fuzzy (IT2FL). On various benchmark image fusion data sets, the uniqueness of the proposed work is tested, and it is found to perform better in terms of Peak Signal Noise Ratio ($PSNR$), Structural Similarity Index Measure ($SSIM$), Edge strength-based Similarity Measure (Q_{ABF}), and Mutual information (MI).

Article information:

Keywords: Image Fusion, Fuzzy Entropy, Novel Improved Firefly Algorithm, Scale Invariant Feature Transform (SIFT), Type-2 Interval Fuzzy

Article history:
Received: December 27, 2022
Revised: April 1, 2023
Accepted: June 24, 2023
Published: June 26, 2023
(Online)

DOI: 10.37936/ecti-cit.2023172.251163

1. INTRODUCTION

Medical imaging is a technique aimed at creating images of the human body using various medical scanners for clinical purposes. These scanned images are provided to physicians and radiologists for diagnosing several disorders and diseases related to the human body. With the advancement in technology, there are many types of medical scanners which provide specific imaging details of the human body. For instance, a Computed Tomography (CT) image scanner provides hard tissue images of the body, such as bones, brain, lungs, etc. At the same time, a Magnetic Resonance Imaging (MRI) scanner provides information about irregularities in soft tissues such as blood vessels of the human body. A PET (Positron Emission Tomography) image scanner can provide functional information about an organ in the human body. While MRI and CT scanners provide anatomical and structural information about the body, the PET scanner can only provide functional information. Thus any one of these image modalities alone is not capable of providing all relevant information of an organ in the human body.

Image fusion can assist physicians and radiologists with more accurate clinical information that may not be possible usually with any one of the imaging modalities discussed above. It is described as a technique for merging data from various imaging modalities to provide an image of a particular organ that is more instructive than individual images produced by the many imaging modalities.This improves the accuracy of diagnosing the disorders or diseases about an organ of the human body, thus enhancing the clinical ability of medical images. Medical image fusion has recently been the subject of a lot of ongoing research [1-3]. Medical image fusion finds its applications in oncology, radiology, ultrasound, cardiac disease diagnosis, etc.

2. RELATED WORKS

In literature, wavelet transforms, including discrete wavelet decomposition (DWT), complex

---

[1] The author is with Usha Rama College of Engineering and Technology,Telaprolu, India., E-mail: sree.02476@gmail.com
[2] The author is with Gudlavalleru Engineering College, Gudlavalleru, India., E-mail: varaprasadvvkd@gmail.com
[3] The author is with Jawaharlal Nehru Technological University, Kakinada, India., E-mail: prasad_kodati@yahoo.co.in

wavelet decomposition (CWT), stationary wavelet decomposition (SWD), and pyramids like the Laplacian pyramid are the most often utilized multiscale image decomposition approaches [4–6]. In [7], the authors surveyed on various discrete wavelet transformed-based image fusion approaches and they contrasted them with the Laplacian pyramid techniques already in use, various wavelet families that were accessible, and various resolution levels. In contrast, [8] discusses numerous classifications of image fusion approaches based on multi-scale decomposition, primarily using wavelet transformation and Laplacian pyramid techniques and their variations. In addition, Image fusion can be carried out using the wavelet, pyramid, Shearlet, contourlet, dual-tree complex wavelet, and Curvelet.

The current pyramid image fusion is outperformed by the discrete wavelet transform-based image fusion, although DWT has issues with shift aliasing, directionality absence, and variance. The dual-tree complex wavelet technique solves these issues and is successfully used for image fusion [13]. Due to the directionality and shift-invariance properties of the dual-tree complex wavelet, the fused image is free of artifacts. Additionally, the wavelet family of techniques generally lacks the ability to represent image curves and edges. Some cutting-edge multiscale geometric analysis algorithms are added to image fusion in order to overcome and emphasize the edges and curves precisely. Curvelets are used to convert images to the frequency domain for improved comprehension [14]. The use of these Curvelets for remote sensing applications is explained in[15]. In addition to contourlet and Curvelet, there is a different transform known as the Non-Subsampled Contourlet Transform, which is superior to changing two-dimensional images and gives images with inherent geometrical structure [16]. In this transform, the image's discontinuities are highlighted by the first Laplacian pyramid, and linear structures are created by combining them with the aid of a directional filter bank. The contourlet transform has been successfully used for applications like surveillance [17], medical imaging [18], and remote sensing [19] due to its effectiveness in describing spatial structures. Shift-invariance is a feature that this contourlet transform does not possess due to the down-sampling process. The Non-Subsampled contourlet transform is the answer to this issue, but it is a labor-intensive process. Moreover, filters employed in contourlet transform are fixed; hence, it fails to represent complex spatial structures in all directions [20].In [21], image fusion is performed with a shearlet transform successfully. Computationally complexity in transforming the image with a Shearlet is less as compared to a contourlet, and it provides unlimited directions for shearing and provides different sizes [22].

In [23], the authors proposed image fusion techniques in multi-scale decompositions based on weighted averages; the authors clearly explained the effect of weights on image fusion quality. They choose local and global weights at different scales. Based on the input images, Gemma Piella first created a multi-resolution segmentation, which she then used to direct the fusion procedure [24]. Lately, Shen et al. proposed image fusion for medical images based on novel cross-scale rule by considering both interscale and intrascale consistencies. Furthermore, the weights at different scales are optimized by using a generalized random walker's method, which effectively exploits the spatial correlation among adjacent pixels [25]. Whereas in [26], Instead of employing a global optimization method, a guided filtering-based weighted average is used for fusion. Finally, it is concluded, fused image quality in multi-scale decomposition depends on the level of decomposition and fusion strategies.

While selecting a method that is appropriate for our application, there is a need to consider several criteria, including strength, direction, ridges, offset of the image borders, and other singularities. Once the technique is chosen, we go forward with global optimization techniques. Global optimization seeks to achieve our aim by identifying the optimal set of permissible conditions. The minima and maxima of continuous and differential functions are discovered using this method. Krill Herd Algorithm (KHA), Particle Swarm Optimization (PSO), Gray Wolf Optimization (GWO), Honey Bee Mate Optimization (HBMO), and Firefly Algorithm are the methodologies (FA). Among them, Firefly has more significant advantages thanks to its straightforward mathematics, simplicity in use, quick convergence, and short processing times.

3. PROPOSED IMAGE FUSION MECHANISM

Although classical FA is easy to implement, for certain problems, it provides unstable performance. One specific reason for the unstable performance of Firefly Algorithm (FA) is that each firefly in FA may be drawn to the brighter fireflies multiple times, which could lead to extreme oscillation. Therefore, to address this drawback, this paper suggested a novel method of image fusion using an improved firefly algorithm (pFA) [42].The attraction of fireflies is significantly less in pFA, which can help simplify computation and improve solution accuracy. The following section provides a more thorough description of the proposed algorithm. With the help of the improved firefly algorithm (pFA), the thresholds were modified, and the outcomes were compared to those obtained using other cutting-edge optimization methods. After the two images have been successfully segmented, the features of the input images are recovered using the best feature extraction algorithms. Texture, edge, and contour are typically considered to be an image's features. Scale Invariant Feature Transform (SIFT) algorithm, created by David Lowe in 1999 [30], is used in this study to extract image features. The SIFT method operates based on the minimal distance between the reference and the object that needs to be detected, which determines the recognition of new things from other images. In reference number [31], the algorithm is described in depth. The retrieved features from the two images are combined using type-2 interval fuzzy fusion rules. In 1965, Zadeh developed the fuzzy set theory [32]. Type-1 fuzzy sets are rigid and not adaptable. To address this problem, a type-2 interval fuzzy set was proposed, which is more flexible in solving uncertainty problems due to its ambiguity in the membership function. As a result, it can be modified to solve known and unknown problems. The flow diagram of the proposed approach is shown in Fig.1.

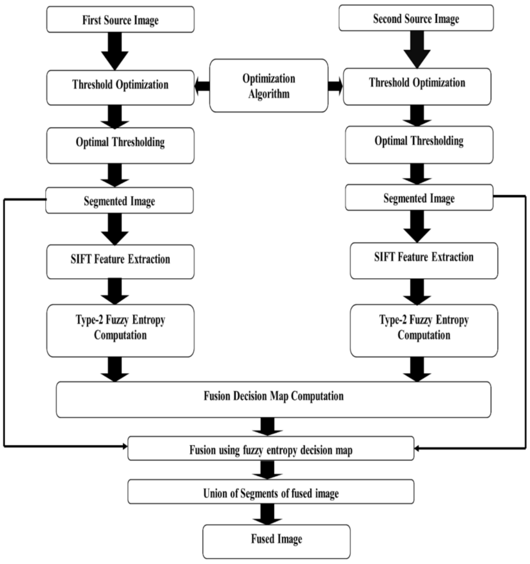

Fig.1: *Flow diagram of the proposed technique.*

The pixel thresholding-based image segmentation methodology is one of the fundamental image segmentation techniques. It is utilized in various applications, including machine vision, data segmentation, data collection, etc., because of its simple and adaptable implementation procedure. Thresholding of an image can be either bi-level or multi-level:bi-level thresholding divides the image into three sections using two thresholds. In contrast, the user selects the number of thresholds in the second instance according to what is needed. The clusters or sections are denoted by "c+1" if "c" stands for the thresholds. To yield a proper segmented result, the source image must be correctly segmented. It can be difficult to set those restrictions for different images. This paper uses an improved firefly method to optimize these thresholds with fuzzy entropy as the objective function. The improved firefly technique, feature extraction using Scale-Invariant Feature Transform(SIFT), the procedure of fuzzy entropy computation, type-2 fuzzy concept , and fusion Rules will all be briefly introduced in the next section.

4. METHODS AND MATERIALS

A quick overview of the concept of fuzzy entropy, the pFA algorithm, the feature extraction procedure using scale-invariant feature transform, the concept of type-2 fuzzy set, and fusion rules are covered in this section.

4.1 Fuzzy entropy

Let 'y' is an event with 'N' elements $\{y_1, y_2, y_3, \ldots, y_N\}$ with respective probabilities $\{P_1, P_2, P_3, \ldots, P_N\}$. Then Shannon entropy H(y) can be defined as $H(Y) = -\sum_{i=1}^{N} P(y_i) \log_b P(y_i)$. Fuzzy entropy, which is considered as an extension of Shannon entropy, is an entropy of a fuzzy set and is defined according to equation (1).

$$H_A^P = -\sum_j^N \mu_A(Y_j) P_j \log(P_j) \tag{1}$$

Here μ_A is the membership function of event A. The equation mentioned above, gives the fuzzy entropy of an uncertain event A with regard to the uncertain distribution P. The same concept can be applied to image thresholding. Let the image gets portioned into three distinguished regions R_d, R_m, and R_b, with corresponding probability distribution function P_d, P_m and P_b by employing two thresholds, T1 and T2.The membership functions (μ) of R_d, R_m, and R_b are μ_d, μ_m, and μ_b, respectively, and require six arguments called a_1,b_1,c_1,a_2,b_2 and c_2. The values of the thresholds T1 and T2 can change depending on the membership functions. After assessing the overall fuzzy entropy, optimal thresholds are computed by using equations (7) and (8). The fuzzy membership functions for a_1=40; b_1=80; c_1=100; a_2=140; b_2=180; c_2=200, and k=0 to 255 are shown in Fig.2 [33].

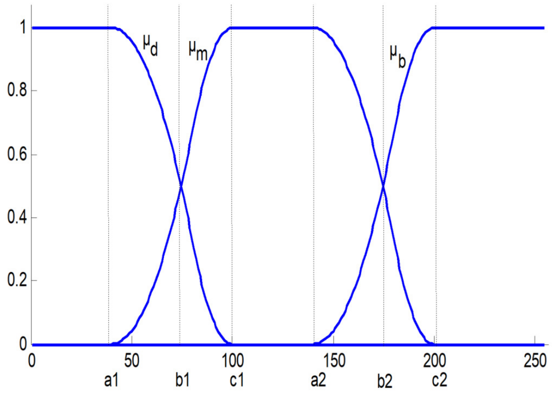

Fig.2: *Membership functions of three distinct regions of an image.*

From Fig.2, the fuzzy membership functions of different regions are defined as per the equations (2),(3), and (4)

$$\mu_m(k)=\begin{cases} 0 & k \le a_1 \\ \dfrac{(k-a_1)^2}{(c_1)-a_1*(b_1-a_1)} & a_1<k\le b_1 \\ 1-\dfrac{(k-c_1)^2}{(c_1-a_1)*(c_1-b_1)} & b_1<k\le c_1 \\ 1 & c_1<k\le a_2 \\ 1-\dfrac{(k-a_2)^2}{(c_2-a_2)*(b_2-a_2)} & a_2<k\le b_2 \\ \dfrac{(k-c_2)^2}{(c_2-a_2)*(c_2-b_2)} & b_2<k\le c_2 \\ 0 & k>c_2 \end{cases} \tag{2}$$

$$\mu_d(k)=\begin{cases} 1 & k \le a_1 \\ 1-\dfrac{(k-a_1)^2}{(c_1-a_1)*(b_1-a_1)} & a_1<k\le b_1 \\ \dfrac{(k-c_1)^2}{(c_1-a_1)*(c_1-b_1)} & b_1<k\le c_1 \\ 0 & k>c_1 \end{cases} \tag{3}$$

$$\mu_b(k)=\begin{cases} 0 & k \le a_2 \\ \dfrac{(k-a_2)^2}{(c_2-a_2)*(b_2-a_2)} & a_2<k\le b_2 \\ 1-\dfrac{(k-c_2)^2}{(c_2-a_2)*(c_2-b_2)} & b_2<k\le c_2 \\ 0 & k>c_2 \end{cases} \tag{4}$$

Knowing the above equations, the fuzzy entropy of each class of objects can be expressed using equations (5) to (7)

$$H_1 = -\sum_{k=0}^{255} \frac{p_k*\mu_d(k)}{p_d} * \ln\left(\frac{p_k*\mu_d(k)}{p_d}\right) \tag{5}$$

$$H_2 = -\sum_{k=0}^{255} \frac{p_k*\mu_m(k)}{p_m} * \ln\left(\frac{p_k*\mu_m(k)}{p_m}\right) \tag{6}$$

$$H_3 = -\sum_{k=0}^{255} \frac{p_k*\mu_b(k)}{p_b} * \ln\left(\frac{p_k*\mu_b(k)}{p_b}\right) \tag{7}$$

The total fuzzy entropy is determined by adding the fuzzy entropies of each region.

$$H(a_1,b_1,c_1,a_2,b_2,c_2) = H_d + H_m + H_b \tag{8}$$

An objective function that has to be optimized using optimization techniques is equation (8). By changing $a_1, b_1, c_1, a_2, b_2, c_2$, optimization approaches maximise or optimize $H(a_1, b_1, c_1, a_2, b_2, c_2)$ function. The following equation is used to calculate threshold values after these values have been optimized.

$$\begin{aligned} \mu_d(T1) = \mu_m(T1) = 0.5 \text{ and} \\ \mu_m(T2) = \mu_b(T2) = 0.5 \end{aligned} \tag{9}$$

From Fig.2, it can be seen that the points T1 and T2 are where the d(k), m(k), and b(k) curves interact. The values of T1 and T2 were obtained using the following relations:

$$\mathrm{T}_1 = \begin{cases} a_1 + \sqrt{(c_1-a_1)*(b_1-a_1)/_2} & (a_1+c_1)/2 \le b_1 \le c_1 \\ c_1 - \sqrt{(c_1-a_1)*(c_1-b_1)/_2} & (a_1 \le b_1) \le (a_1+c_2)/2 \end{cases} \tag{10}$$

$$\mathrm{T}_2 = \begin{cases} a_2 + \sqrt{(c_2-a_2)*(b_2-a_2)/_2} & (a_2+c_2)/2 \le b_2 \le c_2 \\ c_2 - \sqrt{(c_2-a_2)*(c_2-b_2)/_2} & (a_2 \le b_2) \le (a_2+c_2)/2 \end{cases} \tag{11}$$

The two-level thresholding can be expanded to three or more levels or even limited to one level depending on the needs of the researchers. Six parameters must be optimized for two thresholds, and as the threshold levels rise, so do the number of parameters that must be optimized. In this paper, four thresholds are optimized using improved Firefly Algorithm (pFA), and hence it makes use of twelve parameters which are given as $a_1, b_1, c_1, a_2, b_2, c_2, a_3, b_3, c_3, a_4, b_4, c_4$.

4.2 Overview of Firefly Algorithm (FA)

The Firefly Algorithm (FA) is a meta-heuristic algorithm inspired by nature that was first suggested by Yang [35, 36]. This algorithm was created by emulating the flashing illumination patterns that invertebrates like glowworms and fireflies produce. They produce light from their lower abdomen. Glowworms and fireflies produce bioluminescence with various flashing patterns that they utilize to communicate, obtain food, and find mates with other nearby insects.

The classical FA is created by taking into consideration the following factors [37–40]:

1. Each firefly is unisex, and regardless of their sex, they will all be attracted to the nearby firefly.
2. The attractiveness between two fireflies is inversely associated with their brilliance. For every pair of flashing fireflies, the firefly with the greater luminance will draw in the firefly having the lower luminance. Due to a reduction in brightness, the attraction between two fireflies reduces as their distance grows. If there is not another firefly that is brighter than it, a firefly will migrate at random.
3. The objective function's landscape influences or determines a firefly's brightness.

4.3 Parameters of Firefly Algorithm:

The variations in light intensity and attraction between nearby fireflies are the main factors determining how effective the FA is. The increased separation of fireflies will have an impact on these two metrics.

The following Gaussian form can be used to express brightness variation analytically:

$$I(r) = I_0 e^{-\gamma d^2} \tag{12}$$

Where γ is termed as the light absorption coefficient, I is the new light intensity, I_0 is light intensity at $r = 0$. Analytically, the luminance's attractiveness can be expressed as

$$\beta = \beta_0 e^{\gamma d^2} \tag{13}$$

Where β-attraction coefficient and β_0-attractiveness at $r = 0$.

In the n-dimensional search space, the Cartesian distance between two fireflies i and j at X_i and X_j can be expressed mathematically as

$$d_{ij} = \sqrt{\sum\nolimits_{k=1}^{n} (X_{j,k} - X_{j,k})^2} \tag{14}$$

In FA, the inverse square law governs the light intensity at a given distance d from the light source Xi. As the distance d rises, the firefly's light intensity I decrease(since Iα $\frac{1}{d^2}$).The position update equation (12) can be used to predict how the attracted firefly i will move in the direction of a brighter firefly j.

$$X_i(t+1) = X_i(t) + \beta_0 e^{-\gamma d_{ij}^2}[X_i(t) - X_i(t)] + \psi \tag{15}$$

Where $X_i(t+1)$ is the updated position of the firefly $X_i(t)$ is firefly's initial position.

$\beta_0 e^{-\gamma d_{ij}^2}$[$X_i$(t)- X_i(t)] is an attraction between fireflies ψ is a randomization parameter in the range [0,1] and is given as α[rand-0.5].

$$X_i(t+1) = X_i(t) + \psi \tag{16}$$

4.4 Working methodology of Firefly Algorithm

In this section, using a two-dimensional optimization problem, the essential operation of the classical FA is illustrated. Six fireflies are considered to be present in total. The two-dimensional search space contains all the fireflies at random when the algorithm is initialized. In this problem, it is presumable that there are two local best values and one global best value in the search space, as shown in Fig.3.

As shown in Fig. 3(a), some fireflies progress toward the local best (LB) values during the initial search, while others arrive at the global best (GB) value. Firefly 1 ($FF1$) is at LB1, Firefly 4 ($FF4$) is at GB, and Firefly 5 ($FF5$) is at LB2, according to Fig. 3(a). $FF2$, $FF3$, and $FF6$ are located between LB1 and GB, LB2, and GB, respectively. Compared to $FF1$ and $FF5$, $FF4$ produces light that is brighter in intensity. At this point, $FF2$ goes in the direction of LB1 or GB according to the Cartesian distance d_{ij} calculated using equation (11).In this instance, the distance (D1) between $FF1$ and $FF2$ is smaller than it is for $FF2$; hence $FF2$ goes in the direction of LB1. Similar to how $FF3$ is more likely to be drawn to GB than LB2, $FF3$'s Cartesian distance from $FF4$ to $FF3$ (D3) is smaller than D4's. Since the distance between $FF6$ and $FF5$ (D5) is smaller than the distance between $FF6$ and D6 (D6), $FF6$ is probably drawn to LB2.

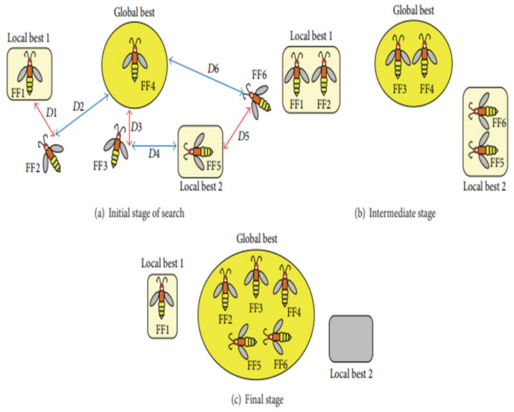

(a) Initial stage of search
(b) Intermediate stage
(c) Final stage

Fig.3: *Working Principle of Firefly Algorithm.*

The second phase of the search process is depicted in Fig. 3(b). The firefly at the GB is preserved as the search iteration increases. As the number of search iterations increases, the attractiveness between the fireflies at the local best value gradually declines, and all fireflies migrate toward the GB. After optimization search, a sizable number of fireflies are finally gathered at the global best value, as shown in Fig.3(c) [43].

4.5 Improved Firefly Algorithm (pFA)

Each firefly in FA can be drawn in by an excessive number of other fireflies, which leads to extreme oscillation. Therefore, to address this drawback, we suggested a better method known as pFA. The attraction of fireflies is much less in pFA, which can help reduce computing time complexity and improve solution accuracy. In pFA, at first, we determine the value of fitness (f_{it}) of each firefly x_i using equation (17).

$$f_{it} = \begin{cases} \dfrac{1}{1 + f(x_i)}, & \text{if } f(x_i) \geq\ 0, \\ 1 + |f(x_i)| & \text{elsewhere} \end{cases} \tag{17}$$

Where $f(x)$ is an objective function. Now, those fitness values larger than x_i' s (specifically, i'th firefly's) are added to a set K. Last but not least, we use the roulette-wheel selection to select its neighbor; the formula is given in equation (18).

$$p_{fit} = \frac{f_{it}(x_k)}{\sum_{x_{t\epsilon k}} fit(x_t)} \tag{18}$$

Equation (18) guarantees that the better the firefly is, the more chances it can have to be selected as a neighbor. Therefore, whichever candidate is chosen will always provide positive guidance to guide xi in the proper direction. This tactic can lessen selection pressure on fireflies while ensuring population diversity and speeding up convergence. However, there is a situation in which xi is the best firefly in the entire population, and no other firefly is superior to it. As a result, it quickly enters the local optimum. Utilizing the knowledge of xi, the opposite learning skill is implemented to handle this situation. Therefore the position update equation (15) of standard firefly algorithm gets modified into equation (19) in the proposed pFA algorithm.

$$x_i(t+1) = \begin{cases} x_i(t) + \beta_0 e^{-\overset{2}{ij}} [x_k(t) - x_i(t)] + \alpha(-0.5) \\ 1 + u - x_i(t) \end{cases} \tag{19}$$

Here u and l are the upper and lower bounds of variables taken as 255 and 0 in the case of grayscale images. x_k is selected with p_{fit} from set K, and random step α is updated using equation (20) with α_0 =0.7 and $\alpha_1 = 0.25$.

$$\alpha_t = \alpha_0 \alpha_{t-1} \tag{20}$$

4.6 Improved Firefly Algorithm for Optimum Threshold Selection

Step 1: Initialization of parameters

a. Initialize β-attraction coefficient, γ-the light absorption coefficient, ψ –randomization parameter, population size, and I_{max} (maximum iterations required).
b. Set the lower and upper threshold boundaries.[must be between 0 and 255 because of 256 gray levels in a gray image].
c. Determine objective function as Maximization of fuzzy entropy from equation (8)
d. Read the input grayscale image, which is to be segmented.

Step 2: Randomly generate the values of variables $a_1, b_1, c_1, a_2, b_2, c_2, a_3, b_3, c_3, a_4, b_4, c_4$ between 0 and 255 for each firefly of improved firefly optimization algorithm, as the gray values of grayscale image lie between 0 and 255.

Step 3: Evaluate the fitness of each firefly using equation (17).

Step 4: If there is a population with the best fitness value, those are selected to make up set K. Select a firefly x_k from set K as a neighbor with probability p_{fit} computed using equation (18).

Step 5: Update the firefly positions based on equation (19)

Step 6: Repeat steps 3 through 5 until the maximum no. of iterations is reached so that fireflies are drawn towards a global solution.

Step 7: Once maximum no. of iterations is reached, the variable values associated with brighter firefly, which is taken as the global best among all fireflies, are taken as optimal values of $a_1, b_1, c_1, a_2, b_2, c_2, a_3, b_3, c_3, a_4, b_4, c_4$.

Step 8: Using the optimal values of step (7), optimal threshold values are computed using (10) and (11).

4.7 Scale-Invariant Feature Transform.

Harris feature detectors are rotation-invariant, meaning that they can detect corners in images both before and after rotation, but they cannot detect angles when an image is scaled. After the image has been enlarged, corners may or may not be angled. Thus, Scale-invariant feature transform (SIFT) [37] was introduced in 2004 to address this drawback. The algorithm goes through 4 steps:

4.7.1 Scale space peak selection: Potential locations for finding features

Specific window sizes are used with various sized artifacts to distinguish key points, and this method is known as scale-space filtering; Laplacian of Gaussian (DoG) variance creates a window with different sizes. The Gaussian value difference is determined by the difference between two Gaussian images (DoGs).

4.7.2 Key point localization: This step is used for accurately identifying the location of the feature key points. After successfully defining the main points in the first step, these points are further optimized for accuracy by producing various window sizes depending on the Taylor series, and after doing so, if the severe position strength obtained is greater than the user-defined threshold (contrast threshold), then find it or otherwise disregard it. Similarly, any unnecessary edges located after Gaussian function discrepancy, these positions are eliminated by a 2×2 Hessian matrix as in the Harris corner detector. Moreover, after setting A and step B, only the leading edges and main points are received.

4.7.3 Orientation assignment: This step is used to assign an orientation to the identified key points In this stage, orientation is traced between the main points based on their size, magnitude, and direction of gradients. Around 36 bins are included in this document to cover the 360 degrees. The maximum value 'H' is determined from the histogram of an image, and if any main point strength reaches 80 percent of H, it will be found in tracing.

4.7.4 Key point descriptor: The main aim of this step is to describe the key point as a high-dimensional vector.The primary point descriptor is obtained via a local gradient created in the three steps above. The gradient knowledge collected is rotated to comply with the key point direction, then weighted by Gaussian with a variation of 1.5 key point size. A set of histograms which are at the center of the key point, are created with this data. A total of 16 histograms are set in a 4×4 grid shape, and each column contains eight orientation bins. Which leads to a size 128 function vector? Such vectors are called SIFT keys, which mark the nearest point in an image. If more than three keys enable a specific function it will be listed for further processing.

4.8 Type-2 Fuzzy Set

Interval type-2 fuzzy set is used to represent the SIFT features of each segment of the source image ${s_p}^I$ that were extracted after the optimal multi-threshold-based segmentation and SIFT feature extraction. At first, the membership function is selected as follows:

$$\mu_p{}^I(i,j) = \frac{1}{1 + \left| \dfrac{s_p{}^I(i,j) - c}{a} \right|^2} \tag{21}$$

In the above relation, I=(I_1,I_2) are the source images, and (i,j) describes spatial co-ordinates of SIFT features. c is the average of (${s_p}^I$), and ‘a’ is the minimum of (${s_p}^I$). p=1,2,3,4,5 denotes the segment number of the source image, which contains five segments as four-level thresholding is used. Now at each position (i,j) of the membership function, lower and upper membership functions μ_L (i,j) and μ_U (i,j) are calculated with $\alpha = 2$ using equations (22) and (23).

$$\mu_{p_L}^{I}(i,j) = [\mu_p{}^I(i,j)]^{\alpha} \tag{22}$$

$$\mu_{p_U}^{I}(i,j) = [\mu_p{}^I(i,j)]^{\frac{1}{\alpha}} \tag{23}$$

By knowing the membership functions, the fuzzy entropy can be computed by using equation (24) Where X is given as X={(x,y)|x= 0 to M-1, y=0 to N-1} denotes a template of size M × N centered at SIFT feature. Using equation (24), fuzzy entropies of each of the SIFT features of source images I_1 and I_2 are computed using equations (25) and (26). Now the maximum rule is used to generate a decision map of each of the segmented regions of source images I1 and I2 as follows:

5. RESULTS AND DISCUSSIONS

The effectiveness of the suggested strategy is assessed through studies on five pairs of images representing various brain illnesses like neoplastic, cerebrovascular, alzheimers, fatal, and sarcoma are used to evaluate how well the suggested technique performs. Further three different stages like, mild, moderate, and severe, of the above diseases are also considered to identify how the suggested technique performs in each stage of the disease. In this paper, fusion results of all three stages are presented for the diseases considered. The medical images used in the research are provided by `https://www.imagefusion.org/` and `http://www.med.harvard.edu/aanlib/home.html`. All the simulations are performed on HP Compaq LE1902X personal computer with Matlab version 2016a.

$$E_p{}^I(i,j) = \sum\nolimits^{\cdot}_{x,y\in X} [\mu_{p_U}^{I}(x,y) - \mu_{p_L}^{I}(x,y)] + \sum\nolimits^{\cdot}_{x,y\in X} \cdot \frac{\min[\mu_{p_L}^{I}(x,y), 1 - \mu_{p_U}^{I}(x,y)]}{\max[\mu_{p_L}^{I}(x,y), 1 - \mu_{p_U}^{I}(x,y)]} \tag{24}$$

$$E_p{}^{I_1}(i,j) = \sum\nolimits^{\cdot}_{x,y\in X} [\mu_{p_U}^{I_1}(x,y) - \mu_{p_L}^{I_1}(x,y)] + \sum\nolimits^{\cdot}_{x,y\in X} \cdot \frac{\min[\mu_{p_L}^{I_1}(x,y), 1 - \mu_{p_U}^{I_1}(x,y)]}{\max[\mu_{p_L}^{I_1}(x,y), 1 - \mu_{p_U}^{I_1}(x,y)]} \tag{25}$$

$$E_p{}^{I_2}(i,j) = \sum\nolimits^{\cdot}_{x,y\in X} [\mu_{p_U}^{I_2}(x,y) - \mu_{p_L}^{I_2}(x,y)] + \sum\nolimits^{\cdot}_{x,y\in X} \cdot \frac{\min[\mu_{p_L}^{I_2}(x,y), 1 - \mu_{p_U}^{I_2}(x,y)]}{\max[\mu_{p_L}^{I_2}(x,y), 1 - \mu_{p_U}^{I_2}(x,y)]} \tag{26}$$

$$\begin{aligned} D_p(i,j) &= 1 \quad if \;\; E_p{}^{I1}(i,j) > E_p{}^{I2}(i,j) \\ &= 0 \qquad\qquad elsewhere \end{aligned} \tag{27}$$

With the help of $D_p(i,j)$, the segments of sources images are combined as given in equation(28)

$$S_p{}^F(i,j) = D_p(i,j)^* S_p{}^{I1}(i,j) + [1 - D_p(i,j)]^* S_p{}^{I2}(i,j) \tag{28}$$

Where $S_p{}^{I1}$ indicates segmented regions of the first source image and $S_p{}^{I2}$ indicates segmented regions of the second source image, and $S_p{}^F$ indicates fused segmented regions.The final fused image $\mathrm{I_F}$ is now obtained by uniting all the fused segmented regions.

$$Fused\ Image,\ I_F = U_{p=1}^{5} S_p{}^F \tag{29}$$

5.1 Performance metrics

Table 1: *Performance Measures*

Performance Metric	Mathematical formulae
Peak Signal to Noise Ratio (PSNR) in dB	$\mathrm{PSNR} = 10\log_{10}\left(\frac{2^r-1}{MSE}\right)^2$ A higher value of PSNR is desired, which indicates good quality fused image.
Mutual Information (MI)	$MI(X,Y) = \sum_{x\in X}\sum_{y\in Y} p(x,y)\log_2 \frac{p(x,y)}{p(x)p(y)}$ $MI_F^{AB} = MI(A,F) + MI(B,F)$ Where MI(A,F) indicates mutual information between the first source image, and the fused image and MI(B,F) indicates mutual information between the second source image and the fused image. A Higher value of MI is recommended for better fusion.
Structural Similarity Index Measure (SSIM)	$SSIM = \frac{(2\mu_a\mu_b + C1)(2\sigma_{ab} + C2)}{(\mu_a{}^2 + \mu_b{}^2 + C1)(\sigma_a{}^2 + \sigma_b{}^2 + C2)}$ The degree of similarity or proximity between two images is determined using the structural similarity index. Its range is [0, 1]. Any value close to 1 indicates good Structural Similarity in the fused image.
Edge Strength (($\mathrm{Q_{ABF}}$))	Its range is [0, 1]. Any value of QABF close to 1 indicates good edge preservation in a fused image. $Q_{ABF} = \frac{\sum_{x=1}^{M}\sum_{y=1}^{N} Q_{AF}(x,y)W_A(x,y) + Q_{BF}(x,y)W_B(x,y)}{\sum_{x=1}^{M}\sum_{y=1}^{N}(W_A(x,y) + W_B(x,y))}$

5.2 Investigations on CT/MRI Image Fusion Neoplastic tumor:

Neoplastic tumors are illnesses that promote the growth of tumors. It is a particular type of tumor brought on by the brain's excessive cell growth. Neoplastic CT and MR images were obtained for this study for different disease phases, such as mild, moderate, and severe, from `www.med.harvard.edu/aanlib/cases/case28/case.html`. Tobacco usage is the leading cause of this tumor. Slice 10 of CT and MR scans represent the mild stage of this disease, Slice 13 represents the moderate stage, and Slice 15 represents the severe stage of this disease.Fig.4 shows fused images of various techniques along with the proposed method for the mild stage of the disease, while Table 2 presents the image quality performance measures for the fused images of the methods considered for all three stages of the disease. In Fig.4, (a) and (b) show CT and MR images of the mild brain tumor connected to a neoplastic illness. The fused images created by the recommended technique using the Krill Herd Optimization and Firefly algorithms are shown in figures (c) and (d), respectively.In contrast, those produced using the pFA with Renyi and Fuzzy entropy objective functions are described in figures (e) and (f) of the same figure. The results of pFA with

Table 2: *Performance metrics for three different stages of neoplastic tumor.*

Stage of the Tumor	**Method**	**PSNR**	**SSIM**	**Q_{ABF}**	**MI**
Mild stage	KHO	34.38	0.955	0.692	3.29
	FA	34.38	0.968	0.697	3.29
	RpFA	34.38	0.947	0.696	3.3
	FpFA	**34.72**	**0.978**	**0.704**	**3.32**
Moderate stage	KHO	34.46	0.956	0.694	3.30
	FA	34.52	0.97	0.702	3.3
	RpFA	34.4	0.965	0.698	3.31
	FpFA	**34.8**	**0.978**	**0.71**	**3.33**
Severe stage	KHO	34.36	0.953	0.692	3.29
	FA	34.42	0.967	0.700	3.29
	RpFA	34.30	0.962	0.696	3.30
	FpFA	**34.70**	**0.975**	**0.708**	**3.32**

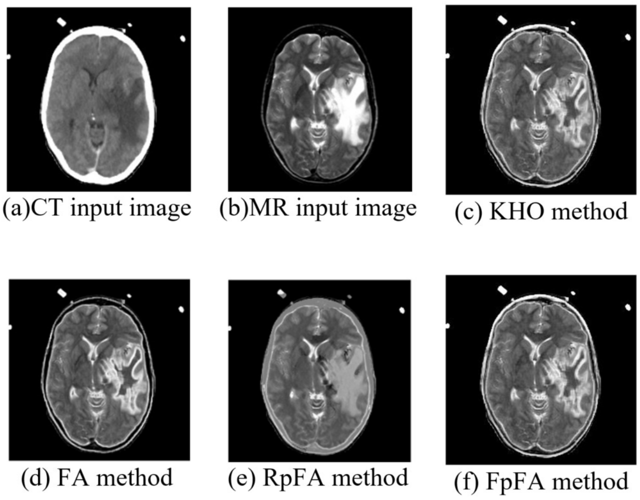
(a)CT input image (b)MR input image (c) KHO method

(d) FA method (e) RpFA method (f) FpFA method

Fig.4: *Fusion results of mild-stage neoplastic tumor.*

Renyi entropy objective function is denoted by RpFA, while that of fuzzy entropy objective function is denoted with FpFA.

Cerebrovascular disease: Cerebrovascular disorders are conditions due to alcohol consumption that can cause strokes and disrupt the blood supply to the brain. For stroke and cerebrovascular disease, hypertension is the main risk factor (high blood pressure).Cerebrovascular CT and MR scanned images of multiple embolic infarctions were obtained for this study for different disease phases such as mild, moderate, and severe from `http://www.med.harvard.edu/aanlib/cases/case34/ct1/014.html`. Slice 10 of CT and MR scans represent the mild stage of this disease, Slice 14 represents the moderate stage, and Slice 16 represents the severe stage of this disease. The (a) and (b) in Fig.5 depict CT and MR images of brain tumors associated with mild cerebrovascular illness. Figures (c) and (d) illustrate the fused images produced by the suggested method using the KHO and Firefly algorithms, respectively, while (e) and (f) of the same figure describe the fused images produced using the pFA with Renyi and Fuzzy entropy objective functions for the mild stage of the disease. Table 3 compares the performance of these methods for three different stages of cerebrovascular tumors using quality assessment metrics such as PSNR, SSIM, QAB/F, and MI.

Alzheimer's disease: Alzheimer's disease is an irreversible, progressive brain disorder that gradually robs people of their memory, thinking abilities, and even their ability to perform basic tasks. Alzheimer MR-PD(proton density) and MR-T2 scanned images were obtained for this study for different disease phases such as mild, moderate, and severe from `http://www.med.harvard.edu/aanlib/cases/case29/mr2/018.html`. Slice 14 of MR-PD and MR-T2 scans represent the mild stage of this disease, Slice 16 represents the moderate stage, and Slice 18 represents the severe stage of this disease. In (a) and (b) of Fig. 6, MR-PD and MR-T2 images of an old man aged 73 years with mild Alzheimer's disease are displayed. The fused images produced by the suggested technique's KHO and Firefly algorithms are shown in figures (c) and (d), respectively. The results obtained utilizing the Renyi and Fuzzy entropy objective functions of the pFA are displayed in (e) and (f) of the same figure for mild stage of alzheimers

Table 3: *Performance metrics for three different stages of cerebrovascular disease.*

Stage of the Tumor	**Method**	**PSNR**	**SSIM**	**Q_{ABF}**	**MI**
Mild stage	KHO	36.56	0.989	0.702	3.54
	FA	34.61	0.966	0.693	3.35
	RpFA	34.6	0.965	0.685	3.35
	FpFA	**36.67**	**0.992**	**0.724**	**3.55**
Moderate stage	KHO	33.63	0.91	0.664	3.25
	FA	33.63	0.892	0.651	3.07
	RpFA	31.77	0.890	0.650	3.06
	FpFA	**33.93**	**0.92**	**0.67**	**3.28**
Severe stage	KHO	30.94	0.892	0.611	2.99
	FA	30.91	0.891	0.610	2.99
	RpFA	30.88	0.890	0.610	2.98
	FpFA	**31.40**	**0.905**	**0.626**	**3.17**

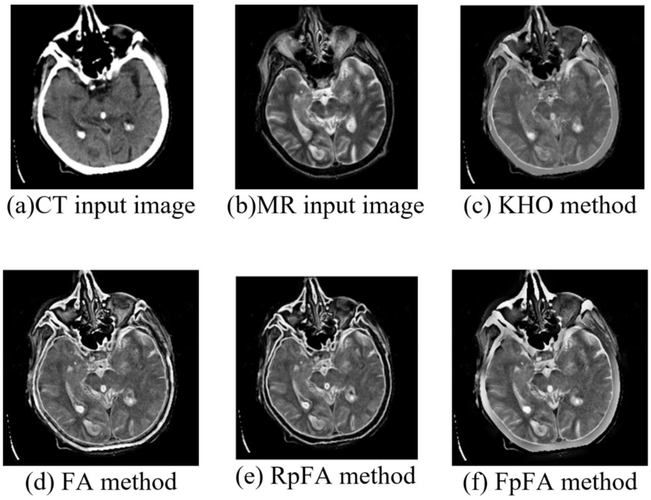
(a)CT input image (b)MR input image (c) KHO method

(d) FA method (e) RpFA method (f) FpFA method

Fig.5: *Fusion results of mild-stage cerebrovascular disease.*

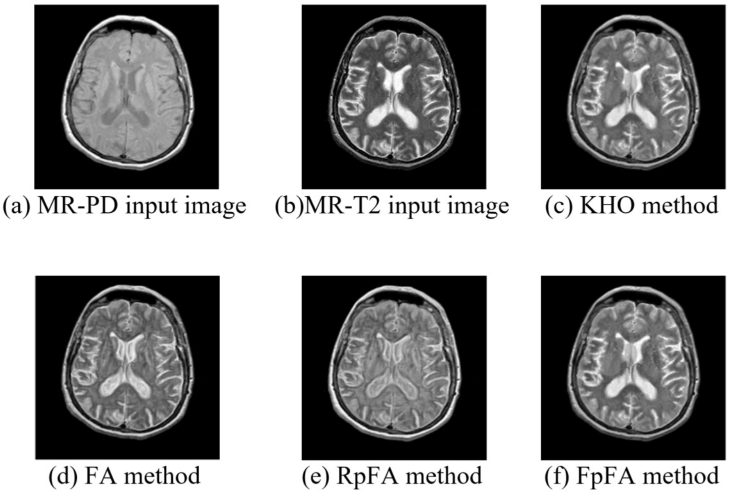
(a) MR-PD input image (b)MR-T2 input image (c) KHO method

(d) FA method (e) RpFA method (f) FpFA method

Fig.6: *Fusion results of mild-stage Alzheimers disease.*

disease. Table 4 compares the performance of these methods for three different stages of alzheimers disease using quality assessment metrics such as PSNR, SSIM, QAB/F, and MI.

Fatal disease: A fatal disease has no treatment and ultimately kills the patient. Depending on the specific ailment, death might take anything from a few hours to several years. Cancer, AIDS, severe heart disease, dementia, etc., are a few fatal diseases. Patients could only receive palliative and supportive care because there is no cure. Fatal MR-T1and MR-T2 scanned images were obtained for this study for

Table 4: *Performance metrics for three different stages of Alzheimers disease.*

Stage of the Tumor	**Method**	**PSNR**	**SSIM**	**Q_{ABF}**	**MI**
Mild stage	KHO	32.85	0.96	0.73	3.12
	FA	32.85	0.952	0.746	3.13
	RpFA	32.87	0.959	0.747	3.17
	FpFA	**33.35**	**0.97**	**0.787**	**3.7**
Moderate stage	KHO	33.97	0.978	0.840	3.59
	FA	34.07	0.981	0.843	3.60
	RpFA	34.17	0.984	0.863	3.64
	FpFA	**34.38**	**0.990**	**0.901**	**4.12**
Severe stage	KHO	34.75	0.979	0.866	4.13
	FA	34.85	0.982	0.869	4.14
	RpFA	34.96	0.985	0.871	4.15
	FpFA	**35.170**	**0.991**	**0.876**	**4.18**

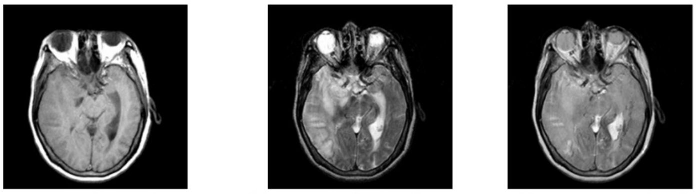

(a) MR-T1 input image (b)MR-T2 input image (c) KHO method

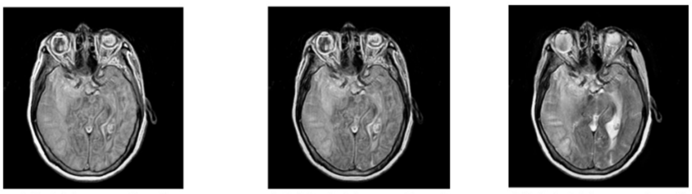

(d) FA method (e) RpFA method (f) FpFA method

Fig.7: *Fusion results of mild-stage fatal disease.*

different disease phases such as mild, moderate, and severe from `http://www.med.harvard.edu/aanlib/cases/case37/mr3/012.html`. Slice 10 of MR-T1 and MR-T2 scans represent the mild stage of this disease, Slice 12 represents the moderate stage, and Slice 14 represents the severe stage of this disease. In (a) and (b) of Fig.7, MR-T1 and T2-Weighted MR images linked to early stages of the deadly disease are shown. The fused images created by the KHO and Firefly algorithms, respectively, are shown in Figures (c) and (d) respectively. The findings obtained utilizing the Renyi and Fuzzy entropy objective functions of the pFA are shown in (e) and (f) of the same figure. Table 5 compares the efficacy of various strategies for three stages of fatal disease using quality evaluation metrics such as PSNR, SSIM, QAB/F, and MI. The improved Firefly algorithm pFA with fuzzy entropy objective function surpassed all competing methods according to performance metrics for each of the three stages of the disease.

Sarcoma disease: A malignant tumor or sarcoma is an uncommon cancer. Fat, muscles, blood vessels, nerves, bones, and cartilage are just a few examples of connective tissue cells where sarcomas can develop. Sarcoma CT and MR scanned images were obtained for this study for different disease phases, such as mild, moderate, and severe, from `http://www.med.harvard.edu/aanlib/cases/case33/ct1/020.html`. Slice 17 of CT and MR-T2 scans represent the mild stage of this disease, Slice 19 represents the moderate stage, and Slice 20 represents the severe stage of this disease. In (a) and (b) of Fig.8, CT and MR images of a patient with a mild stage of sarcoma disease are displayed. Figures (c) and (d) of the Fig.8 describes the fused images obtained from the suggested methodology using the KHO and Firefly algorithms. In contrast, (e) and (f) of the same figure represent the fused images produced using the Renyi and Fuzzy entropy objective functions of the pFA.

Using quality evaluation criteria such as PSNR, SSIM, QAB/F, and MI, Table 6 evaluates the effectiveness of several techniques for three distinct stages of sarcoma illness. Performance measurements for each of the three stages of the disease showed that the improved Firefly algorithm pFA with fuzzy entropy objective function outperformed all competing approaches. The graphical analysis of performance

Table 5: *Performance metrics for three different stages of fatal disease.*

Stage of the Tumor	**Method**	**PSNR**	**SSIM**	**Q_{ABF}**	**MI**
Mild stage	KHO	32.80	0.939	0.784	3.61
	FA	32.81	0.936	0.776	3.62
	RpFA	32.89	0.932	0.774	3.6
	FpFA	**34.42**	**0.968**	**0.877**	**4.1**
Moderate stage	KHO	33.09	0.946	0.790	3.94
	FA	33.04	0.943	0.781	3.65
	RpFA	33.12	0.939	0.779	3.63
	FpFA	**34.66**	**0.975**	**0.883**	**4.13**
Severe stage	KHO	33.65	0.965	0.806	4.01
	FA	33.70	0.961	0.797	3.72
	RpFA	33.78	0.957	0.795	3.70
	FpFA	**35.36**	**0.994**	**0.901**	**4.21**

Table 6: *Performance metrics for three different stages of sarcoma disease.*

Stage of the Tumor	**Method**	**PSNR**	**SSIM**	**Q_{ABF}**	**MI**
Mild stage	KHO	33.81	0.923	0.669	2.9
	FA	33.86	0.925	0.679	2.96
	RpFA	33.8	0.928	0.674	2.9
	FpFA	**34.54**	**0.944**	**0.693**	**3.04**
Moderate stage	KHO	32.12	0.877	0.636	2.76
	FA	32.17	0.879	0.645	2.81
	RpFA	32.11	0.882	0.640	2.76
	FpFA	**32.81**	**0.897**	**0.658**	**2.94**
Severe stage	KHO	30.80	0.841	0.609	2.64
	FA	30.85	0.843	0.619	2.70
	RpFA	30.79	0.877	0.614	2.64
	FpFA	**31.46**	**0.892**	**0.631**	**2.82**

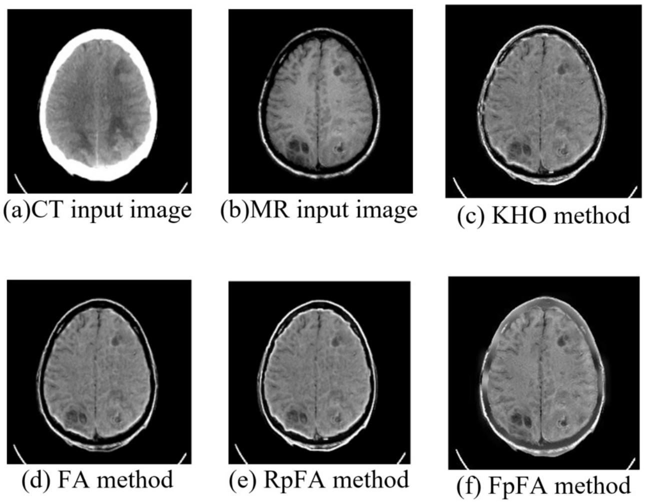
(a)CT input image (b)MR input image (c) KHO method
(d) FA method (e) RpFA method (f) FpFA method

Fig.8: *Fusion results of mild-stage sarcoma disease.*

metrics for various diseases is presented in (a),(b),(c), and (d) of Figure 9.

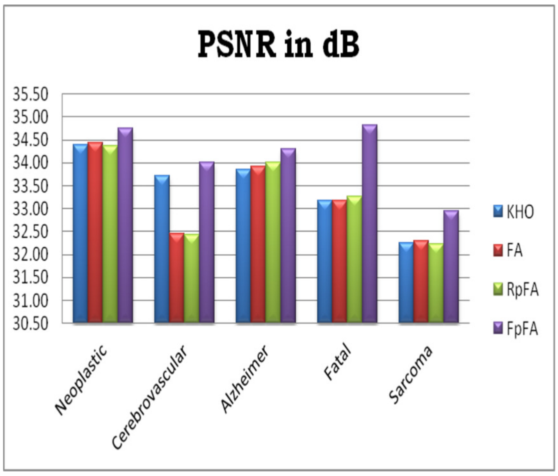

Fig.9(a): *Analysis of average PSNR of three stages of each disease.*

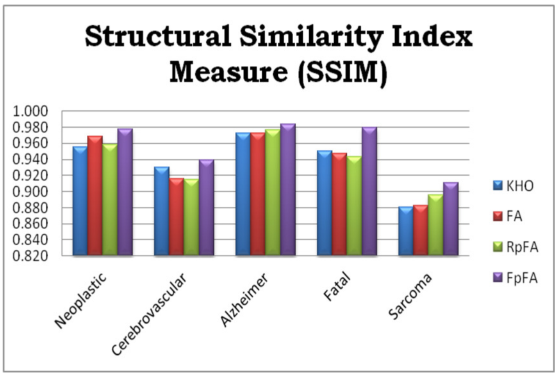

Fig.9(b): *Analysis of average SSIM of three stages of each disease.*

Analysis of PSNR of FpFA shows an improvement of 8 to 16% in PSNR for the FpFA method for neoplastic disease than existing methods, while there is a 1 to 2% improvement to other optimization techniques considered in the proposed fusion methodology. For cerebrovascular disease, FpFA produced a 19 to 26% improvement over existing methods while providing a 1.5 to 11% improvement over other optimization techniques considered in the proposed fusion methodology. For alzheimers disease, FpFA offered a 3 to 6% improvement in PSNR than existing methods while offering 0.5 to 3% improvement to other optimization techniques considered in the proposed fusion methodology. In the case of a fatal disease, FpFA improved PSNR by 6 to 12% more than existing methods while improving PSNR by 4 to 6% more than other optimization techniques considered in the proposed fusion methodology. For sarcoma disease, FpFA produced a 3 to 10% improvement in PSNR than existing methods while offering a 2 to 3% improvement to other optimization techniques considered in the proposed fusion methodology.

Analysis of SSIM of FpFA shows an improvement of 8 to 21% in SSIM for the FpFA method for neoplastic disease than existing methods, while there is a 1 to 7% improvement than other optimization techniques considered in the proposed fusion methodology. For cerebrovascular disease, FpFA produced a 6 to 36% improvement over existing methods while providing a 1 to 12% improvement over other optimization techniques considered in the proposed fusion methodology. For alzheimers disease, FpFA offered a 9.5 to 22% improvement in SSIM than existing methods while offering a 1 to 9% improvement over other optimization techniques considered in the proposed fusion methodology. In the case of a fatal disease, FpFA improved SSIM by 20 to 27% than existing methods while improving SSIM by 3 to 8% than other optimization techniques considered in the proposed fusion methodology. For sarcoma disease, FpFA produced a 2 to 12% improvement in SSIM than existing methods while offering a 3 to 6% improvement to other optimization techniques considered in the proposed fusion methodology.

From the analysis of QABF of FpFA,it is revealed that there is an improvement of 7 to 76% in Q_{ABF} for the FpFA method for neoplastic disease than existing methods.In comparison, there is a 2 to 24% improvement than other optimization techniques considered in the proposed fusion methodology.For cerebrovascular disease, FpFA produced an improvement of 18 to 78% over existing methods while providing a 2 to 28% improvement over other optimization techniques considered in the proposed fusion methodology.For alzheimers disease, FpFA offered a 21 to 74% improvement in QABF than existing methods while offering a 5 to 19% improvement over other optimization techniques considered in the proposed fusion methodology. In the case of a fatal disease, FpFA improved QABF by 35 to 70% more than existing methods while improving QABF by 11 to 18% more than other optimization techniques considered in the proposed fusion methodology. For sarcoma disease, FpFA produced a 10 to 68% improvement in QABF than existing methods while offering a 6 to 7% improvement to other optimization techniques considered in the proposed fusion methodology.

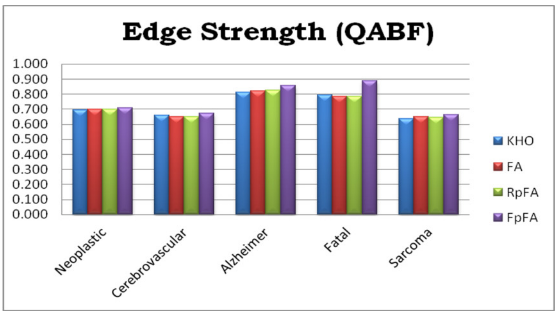

Fig.9(c): *Analysis of average QABF of three stages of each disease.*

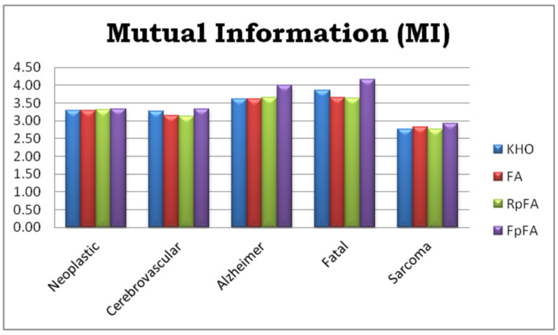

Fig.9(d): *Analysis of average MI of three stages of each disease.*

Analysis of MI of FpFA shows that, there is an improvement of 4 to 19% in MI for the FpFA method for neoplastic disease than existing methods, while there is a 1 to 12% improvement to other optimization techniques considered in the proposed fusion methodology.For cerebrovascular disease, FpFA produced a 14 to 65% improvement over existing methods while providing a 2 to 14% improvement over other optimization techniques considered in the proposed fusion methodology.For alzheimers disease, FpFA offered a 19 to 56% improvement in MI than existing methods while offering a 10 to 30% improvement over other optimization techniques considered in the proposed fusion methodology. In the case of a fatal disease, FpFA improved MI by 12 to 47% more than existing methods while improving MI by 8 to 12% more than other optimization techniques considered in the proposed fusion methodology. For sarcoma disease, FpFA produced an 8 to 21% improvement in MI than existing methods while offering a 4 to 15% improvement to other optimization techniques considered in the proposed fusion methodology.

6. CONCLUSIONS

Two MRI / CT and MRI images have been combined in this study to identify illnesses like a neoplastic tumor, Alzheimer's disease, cerebrovascular disease, sarcoma tumor, and fatal tumor. Both input images are segmented using a 2-D histogram and proposed novel Firefly Algorithm, with the premise that fuzzy entropy acts as an objective function. Scale Invariant Feature Transform (SIFT) is used to extract the features of the segmented portions of both source images. Type-2 interval-based fuzzy entropy is then used as the decision rule to combine the source images. From the quantitative and qualitative results, it is evident that the pFA-based fusion technique outperforms the other optimization techniques that were taken into consideration for diagnosing the various brain tumors.

References

[1] Y. Liu, X. Chen, Z. Wang, Z. J. Wang, R. K. Ward and X. Wang, “Deep learning for pixel-level image fusion: Recent advances and future prospects,” *Information Fusion*, vol. 42, pp. 158-173, 2018.

[2] B. Rajalingam and R. Priya, “Hybrid multimodality medical image fusion technique for feature enhancement in medical diagnosis,” *International Journal of Engineering Science Invention (IJESI)*, vol. 2, pp. 52-60, 2018.

[3] J. Ma, Y. Ma and C. Li, “Infrared and visible image fusion methods and applications: A survey,” *Information Fusion*, vol. 45, pp. 153-178, 2019.

[4] L. Tan, Y. Chen and W. Zhang, “Multi-focus Image Fusion Method based on Wavelet Transform,” in *Journal of Physics: Conference Series*, vol. 1284, no. 1, p. 012068, August 2019.

[5] R. Singh and A. Khare, “Fusion of multimodal medical images using Daubechies complex wavelet transform–A multiresolution approach,” *Information Fusion*, vol. 19, pp. 49-60, 2014.

[6] F. Vollnhals, J. N. Audinot, T. Wirtz, M. Mercier-Bonin, I. Fourquaux, B. Schroeppel,U. Kraushaar, V. Lev-Ram, M. H. Ellisman and S. Eswara, “Correlative microscopy combining secondary ion mass spectrometry and electron microscopy: comparison of intensity–hue–saturation and Laplacian pyramid methods for image fusion,” *Analytical chemistry*, vol. 89, no. 20, pp. 10702-10710, 2017.

[7] K. Amolins, Y. Zhang and P. Dare, “Wavelet based image fusion techniques—An introduction, review and comparison,” *ISPRS Journal of photogrammetry and Remote Sensing*, vol. 62, no. 4, pp. 249-263, 2007.

[8] J. Chen, X. Li, L. Luo, X. Mei and J. Ma, “Infrared and visible image fusion based on target-enhanced multiscale transform decomposition,” *Information Sciences*, vol. 508, pp. 64-78, 2020.

[9] L. Wang, B. Li and L. F. Tian, “Multi-modal medical image fusion using the inter-scale and intra-scale dependencies between image shift-invariant shearlet coefficients,” *Information Fusion*, vol. 19, pp. 20-28, 2014.

[10] H. Li, Y. Chai and Z. Li, “Multi-focus image fusion based on nonsubsampled contourlet transform and focused regions detection,” *Optik*, vol. 124, no.1, pp. 40-51, 2013.

[11] B. Sun, W. Zhu, C. Luo, K. Hu, Y. Hu and J. Gao, “Fusion of noisy images based on joint distribution model in dual-tree complex wavelet domain,” *International Journal of Imaging Systems and Technology*, vol. 29, no. 1, pp. 29-41, 2019.

[12] B. Yang and S. Li, “Pixel-level image fusion with

simultaneous orthogonal matching pursuit," *Information fusion*, vol. 13, no.1, pp. 10-19, 2012.

[13] J. J. Lewis, R. J. O'Callaghan, S. G. Nikolov, D. R. Bull and N. Canagarajah, "Pixel-and region-based image fusion with complex wavelets. Information fusion, 8(2), 119-130, 2007.

[14] E. J. Candès and D. L. Donoho, "Curvelets and curvilinear integrals," *Journal of Approximation Theory*, vol. 113, no. 1, pp. 59-90, 2001.

[15] N. Kaur, M. Bahl and H. Kaur, "Review on: image fusion using wavelet and curvelet transform," International Journal of Computer Science and Information Technologies (IJCSIT), vol.5., no. 2, pp. 2467-2470, 2014.

[16] H. Li, Y. Chai and Z. Li, "Multi-focus image fusion based on nonsubsampled contourlet transform and focused regions detection," *Optik*, vol. 124, no.1, pp. 40-51, 2013.

[17] Q. Zhang and X. Maldague, "An adaptive fusion approach for infrared and visible images based on NSCT and compressed sensing, *Infrared Physics & Technology*, vol. 74, pp. 11-20, 2016.

[18] L. Tang, J. Qian, L. Li, J. Hu and X. Wu, "Multimodal medical image fusion based on discrete T chebichef moments and pulse coupled neural network," *International Journal of Imaging Systems and Technology*, vol. 27, no. 1, pp. 57-65, 2017.

[19] Q. Miao, R. Liu, Y. Wang, J. Song, Y. Quan and Y. Li, "Remote sensing image fusion based on shearlet and genetic algorithm," *International Journal of Bio-Inspired Computation*, vol. 9, no.4, pp. 240-250, 2017.

[20] K. P. Upla, M. V. Joshi and P. P. Gajjar, "An Edge Preserving Multiresolution Fusion: Use of Contourlet Transform and MRF Prior," in *IEEE Transactions on Geoscience and Remote Sensing*, vol. 53, no. 6, pp. 3210-3220, June 2015.

[21] L. Wang, B. Li and L. F. Tian, "Multi-modal medical image fusion using the inter-scale and intra-scale dependencies between image shift-invariant shearlet coefficients," *Information Fusion*, vol. 19, pp. 20-28, 2014.

[22] K. J. Xia, H. S. Yin and J. Q. Wang, "A novel improved deep convolutional neural network model for medical image fusion," *Cluster Computing*, vol. 22, no. 1, pp. 1515-1527, 2019.

[23] D. F. Wu, W. He, S. Lin, B. Han and C. S. Zee, "Using real-time fusion imaging constructed from contrast-enhanced ultrasonography and magnetic resonance imaging for high-grade glioma in neurosurgery," *World neurosurgery*, vol. 125, pp. e98-e109,2019.

[24] J. Ma, W. Yu, P. Liang, C. Li and J. Jiang, "FusionGAN: A generative adversarial network for infrared and visible image fusion. Information Fusion, vol. 48, pp. 11-26, 2019.

[25] R. Shen, I. Cheng and A. Basu, "Cross-scale coefficient selection for volumetric medical image fusion," *IEEE Transactions on Biomedical Engineering*, vol. 60, no. 4, pp. 1069-1079, 2012.

[26] U. N. Dulhare and A. M. Khaleed, "Taj-Shanvi Framework for Image Fusion Using Guided Filters," *Data Management, Analytics and Innovation*, Springer, Singapore, pp. 419-427, 2020.

[27] X. S. Yang, *Nature-Inspired Metaheuristic Algorithms*, Luniver Press, 2008.

[28] J. Kennedy and R. Eberhart, "Particle swarm optimization," *Proceedings of ICNN'95 - International Conference on Neural Networks*, Perth, WA, Australia, vol.4, pp. 1942-1948, 1995.

[29] D. T. Pham and M. Castellani, "The Bees Algorithm: Modelling Foraging Behaviour to Solve Continuous Optimization Problems," *Proc. Ime che*, vol. 223, no. 12, pp. 2919-2938, 2009.

[30] D. G. Lowe, "Object recognition from local scale-invariant features," *Proceedings of the Seventh IEEE International Conference on Computer Vision*, Kerkyra, Greece, vol.2, pp. 1150-1157, 1999.

[31] Y. He, G. Deng, Y. Wang, L. Wei, J. Yang, X. Li and Y. Zhang, "Optimization of SIFT algorithm for fast-image feature extraction in line-scanning ophthalmoscope," *Optik*, vol. 152, pp. 21-28, 2018.

[32] L. A. Zadeh, "Fuzzy sets," *Information and Control*, vol. 8, no. 3, pp. 338–353, 1965.

[33] S. Pare, A. K. Bhandari, A. Kumar, G. K. Singh, "A new technique for multilevel color image thresholding based on modified fuzzy entropy and Lévy flight firefly algorithm," *Computers & Electrical Engineering* vol. 70, pp. 476–495, 2018.

[34] A. H. Gandomi, X. S. Yang and A. H. Alavi, "Cuckoo search algorithm: A metaheuristic approach to solve structural optimization problems," *Engineering with Computers*, vol. 29, no. 1, pp. 17–35, 2013.

[35] E. E. Hofmann,, A. E. Haskell,, J. M. Klinck and C. M. Lascara, "Lagrangian modelling studies of Antarctic krill (Euphausia superba) swarm formation," *ICES Journal of Marine Science*, vol. 61, no. 4, pp. 617–631, 2004.

[36] H. J. Price, "Swimming behavior of krill in response to algal patches: A mesocosm study," *Limnology and Oceanography*, vol. 34, no. 4, pp. 649–659, 1989.

[37] C. Harris and M. Stephens, "A Combined Corner and Edge Detector," *Alvey Vision Conference 15*, Plessey Research Roke Manor, United Kingdom, pp. 147-152, 1988.

[38] Qilian Liang and J. M. Mendel, "Interval type-2 fuzzy logic systems: theory and design," in *IEEE Transactions on Fuzzy Systems*, vol. 8, no. 5, pp. 535-550, Oct. 2000.

[39] J. M. Mendel and R. I. B. John, "Type-2 fuzzy

sets made simple," in *IEEE Transactions on Fuzzy Systems*, vol. 10, no. 2, pp. 117-127, April 2002.

[40] Y. Yang, Y. Que, S. Huang and P. Lin, "Multimodal Sensor Medical Image Fusion Based on Type-2 Fuzzy Logic in NSCT Domain," in *IEEE Sensors Journal*, vol. 16, no. 10, pp. 3735-3745, May 15, 2016.

[41] L. Li and D. Li, "Fuzzy entropy image segmentation based on particle swarm optimization," *Progress in Natural Science*, vol. 18, no. 9, pp. 1167–1171, 2008.

[42] M. V. Srikanth, V. V. K. D. V. Prasad and K. S. Prasad, "An Improved Firefly Algorithm-Based 2-D Image Thresholding for Brain Image Fusion," *International Journal of Cognitive Informatics and Natural Intelligence*, vol. 14 , no. 3 ,July-September 2020.

[43] M. V. Srikanth, V. V. K. D. V. Prasad and K. S. Prasad, "Optimal Threshold Based Brain Image Fusion for Brain Cancer Detection using Firefly algorithm," *International Journal of Recent Technology and Engineering (IJRTE)*, vol. 8, no. 2, pp. 2277-3878, July 2019.

M. V. Srikanth is a Research Scholar, pursuing Ph.D. in the field of Image Processing from Jawaharlal Nehru Technological University, Kakinada,Andhra Pradesh, India. He has been working as an Academician in the capacity of an Assistant Professor in Electronics and Communication department of Usha Rama College of engineering and technology, a reputed Autonomous Engineering College in Andhra Pradesh, India. Apart from regular Academia, the zeal to explore new technologies and a penchant towards pursuing research in the field of Image Processing has made him to do the research work in a governmental organization in Andhra Pradesh. His keen interests are inclined more towards Signal Processing and Embedded Systems.

V. V. K. D. V. Prasad working as a Professor of Electronics & Communication Engineering and convener IQAC in Gudlavalleru Engineering College, an Autonomous NBA accredited College in Andhra Pradesh, India. He received Ph.D. for his work in Signal Processing in 2011 from Jawaharlal Nehru technological University, Kakinada, India. His areas of Interest include Signal Processing, Electrostatics, Electromagnetic fields and Transmission lines. He developed an abstract technical trait that addresses various other fields where digitalization can be achieved. His research findings are in the methodology used, problems encountered and the practical implications of composite features and filtering coefficients in advanced filters.

K. Satya Prasad received B.Tech. (ECE) degree from JNT University, Hyderabad, Andhra Pradesh, India in 1977, M.E. (Communication systems) from University of Madras, India in 1979, Ph.D. from IIT-Madras, India in 1989. He has more than 35 years of experience in teaching and 20 years in R&D. His current research interests include Signals & Systems, Communications, Digital signal processing, RADAR and Telemetry. He worked as Professor of Electronics & Communication Engineering & Former RECTOR, JNTUK and former Pro-Vice Chancellor, KLEF. He also worked as professor of ECE and Rector, Vignan's Foundation for Science, Technology and Research (Deemed to be University), Vadlamudi, Andhra Pradesh. He received patent for his research work in 2015.